Tanzania Journal of Science 50(3): 522-540, 2024
ISSN 0856-1761, e-ISSN 2507-7961

Adsorptive Performance of Composite of Sugarcane Bagasse Fibres and Multiwalled Carbon Nanotubes for Simultaneous Removal of Multi–pollutants from Wastewaters

Joseph W Sengasu, Joseph YN Philip and Kessy F Kilulya
Department of Chemistry, University of Dar es Salaam, Dar es Salaam, Tanzania
Corresponding Author, joseph.wilson393@gmail.com, +255 755 787 874
Received 13 February 2024, Revised 21 July 2024, Accepted August 30, Publ. 30 Sept. 2024
https://dx.doi.org/10.4314/tjs.v50i3.9

Abstract

This paper reports on the performance of the prepared Sugarcane Bagasse Fibres – Multiwalled Carbon Nanotubes (SBF–MWCNTs) composite for simultaneous removal of Crystal Violet (CV), Pb(II), Cr(III), Cd(II) and Co(II) from the effluent using a fixed bed method. Different composites of SBF–MWCNTs biosorbent were prepared from mixtures of varied ratios of SBF and MWCNTs at 25 °C. The SBF–MWCNTs materials were characterized by FT-IR spectroscopy and thermogravimetric analysis. Crystallinity index and swelling behaviour of the materials were also determined. Thomas model linear equation was applied in the assessment of pollutants adsorption performance at different conditions. With a column height of 8 cm containing 1.5 g of SBF–MWCNTs, flow rate of 2.5 mL min^{-1}, pH > 6, and pollutant initial concentrations of ≤25 mg/L, the SBF–MWCNTs composite containing 2% MWCNTs had higher pollutants adsorption capacity (mg/L), 6.61 ± 0.092 Pb(II), 4.78 ± 0.132 CV, 4.58 ± 0.080 Cr(III), 4.09 ± 0.181 Cd(II), 2.98 ± 0.230 Co(II). Whereas, that of unmodified fibres (SBF) were 5.53 ± 0.056 Pb(II), 4.48 ± 0.091 CV, 3.77 ± 0.072 Cr(III), 3.41 ± 0.050 Cd(II) and 2.42 ± 0.031 Co(II). Statistical analysis at 0.05 significance level has shown that adsorption capacity of each contaminant by the SBF–MWCNTs is significantly higher than that of SBF. These results indicate that SBF–MWCNTs composite is a potential biosorbent for the removal of multi–pollutants from aqueous systems.

Keywords: Wastewater treatment; Multi–pollutants; Carbon nanotubes; Sugarcane bagasse; Fixed bed

Introduction

Various pollutants (both inorganic and organic) released from domestic and industrial activities contaminate the environment. Inorganic pollutants such as cadmium, lead, cobalt, chromium, mercury, nickel, anions, acids and alkalis are commonly found in environmental samples. Anthropogenic sources of these pollutants include industrial applications, mining operations, agriculture practices and urbanization (Akhtar et al. 2021). Organic pollutants such as dyes, pesticides, detergents, phenols, polychlorinated biphenyls and trihalomethanes generally originate from activities such as petroleum refinery, pesticides use, manufacturing of paints, textile, electrical appliances, pulp and paper industry, food processing wastes and drinking water treatment plants (Obinnaa and Ebere 2019). The undesirable consequences of environmental pollution are many and broad, ranging from causing adverse health effects to hindering of economic growth (Fang et al. 2021). Although air, soil and aquatic environments can concurrently be polluted, the latter have received considerable attention because large quantities of both soil and air pollutants find their way to water bodies (*i.e.*, groundwater, rivers, lakes and

oceans) through precipitation, leaching and runoff (Akhtar et al. 2021).

Since treatment of pollutant–contaminated water for various activities is inevitable, different techniques have been established with main considerations of simplicity of use and being cost-effective during their development. Numerous approaches are currently applied for the removal of pollutants from wastewater: chemical precipitation (Pohl 2020) ion exchange (Kaleta et al. 2018), membrane separation (Hezarjaribi et al. 2021), photo−catalysis (Liu et al. 2016), solvent extraction, evaporation (Ghurye et al. 2021), electrochemical coagulation (Rincòn and Motta 2014), reverse osmosis (Lopera et al. 2019) and electrodialysis (Choi et al. 2015). Most of these methods are not cost-effective and also not so efficient. Adsorption methods using biosorbents is the most reasonable choice when the two requirements are considered. Researches have proved the efficacy of some agricultural wastes for metal and dye adsorption. Hossain and Hossain (2014) and Shrestha et al (2012) used spent tea leaves to remove malachite green and Pb(II) with Zn(II) ions from aqueous solution, respectively. Mango leaves was applied to remove Cu(II) ions (Ong et al. 2013) and crystal violet (Patil et al. 2011). Al-Azabi et al. (2018) used orange peels for the removal of methylene blue and crystal violet dyes.

The examples mentioned in the preceding paragraph is evidence that numerous researchers analyse one pollutant per method despite the fact that, in nature, the aquatic systems are contaminated by more than one pollutant species (both organic and inorganic). Batch method is commonly preferred because it is easy and cheap to apply, but does not comply with industrial application in comparison to the continuous (fixed bed) method (Patel 2019). Extracts from sugarcane bagasse has been used by different researchers as adsorbent in both batch and continuous method. However, the modification of SBF with MWCNTs for pollutants adsorption has not been reported. This paper reports on the adsorption performance of SBF–MWCNTs for the removal of Pb(II), Cr(III) Cd(II) Co(II) and crystal violet dye from aqueous effluents using continuous fixed bed method.

Materials and Methods

SB was collected from Mtibwa Sugar Company in Morogoro region, Tanzania. About 1 kg of SB was washed with distilled water, dried at 70 °C to a constant weight. The materials were then pulverized and sieved to particle size less than 250 µm. Hydrogen peroxide, sodium hydroxide, hydrochloric acid, nitric acid, cadmium nitrate, lead nitrate, cobalt nitrate, chromium nitrate nonahydrate, crystal violet dye and MWCNTs (95% pure) with diameter range between 50 to 90 nm were all bought from Sigma Aldrich Germany, received from Labequip agent in Dar es Salaam.

Preparation of SBF based adsorbent

The SBF were obtained by delignification which was performed using alkaline hydrogen peroxide as reported by Ma'ruf et al. (2017). About 20 g of ground SB with particle size less than 250 µm was transferred into a 500 mL flask, then 250 mL of 1.0 M H_2O_2 was added. A solution of 2 M NaOH was also added until a pH of 11 was attained. The contents were stirred while heated on a hot plate at 100 °C for 1.5 hours. The contents were left to cool to room temperature, then filtered through Whatman filter paper with pore size of 11 µm. The fibres were washed with methanol and oven dried at 80 °C to constant weight.

Approximately 1.5 g of MWCNTs was purified with 100 mL of 8 M HNO_3 in a round bottomed flask. The mixture was refluxed at 120 °C for 3 hours. Thereafter, the mixture was allowed to cool to 25 °C. A Whatman filter paper of 11 µm pore size was used to recover the purified MWCNTs, washed to pH 7.0 and oven dried at 60 °C to constant weight. About 0.01 g of MWCNTs was dispersed in water followed by about 2.0 g of SBF to make a 0.5% MWCNTs in SBF. The contents were stirred for 30 min. The blended material was obtained by filtering the content through Whatman filter paper of 11 µm pore size. The blended material was dried in a hot air oven at 60 °C to constant weight.

Other composite materials containing 1%, 1.5%, 2%, 2.5%, 3%, 4% and 5% of the MWCNTs in SBF were made in the same way, except that different corresponding weights of MWCNTs were used. The obtained SBF–MWCNTs composite material looks like as seen in a photograph shown in Figure 1.

Figure 1: A photograph showing the likeness of the prepared SBF–MWCNTs composite

FT–IR spectroscopy characterization of both SBF and SBF–MWCNTs was performed using Alpha–Attenuated Total Reflectance (ATR) FT–IR spectrophotometer, Bruker optic GmbH 2011, USA model. Spectra were recorded from 4000 to 650 cm^{-1} in transmittance mode with 4 scans per spectrum at a resolution of 4 cm^{-1}. Boehm titration was performed to determine surface basic and acidic oxygen functional groups on both the unmodified and modified fibres using 0.10 M HCl and 0.10 M NaOH. Thermal stability of the SBF and the corresponding modified SBF–MWCNTs was determined using Bruker TGA 4000 Thermogravimetric Analyser. About 10 mg sample aliquot was placed in a sample holder pan and a TGA curve was recorded at temperatures ranging between 29 °C and 550 °C at a ramp-up rate of 5 °C min^{1}. Crystallinity index was performed using XRD Bruker AXS (Germany), with operating condition of 40 kV and 30 mA, with CuKα radiation wavelength of λ = 15.406 nm. Data were collected from a range of 1° to 40° on a 2θ scale with a speed of 10° min^{-1} and measuring every 0.02 s. Swelling behaviour of the prepared adsorbent materials was performed in water as a solvent, since the materials were designed for use in aqueous medium. About 0.3 g of the materials was soaked in water at 25 °C for 24 h. The swollen fibres were first blotted with filter paper and weighed. The solvent uptake ratio of the fibres was then calculated.

Adsorption performance of the SBF based adsorbents

Up flow of effluent through the fixed bed column was carried out to determine simultaneous adsorption capacity of the contaminants to the SBF–MWCNT composites. Figure 2 shows a sketch of the experimental setup. The experimental setup consisted of sandwiched adsorbent particles in two layers of glass wool immobilised by perforated plates at the bottom and top of the fixed bed column. The packing of the dry adsorbent particles in the column was done by tap-fill method as per Dingenen (1998).

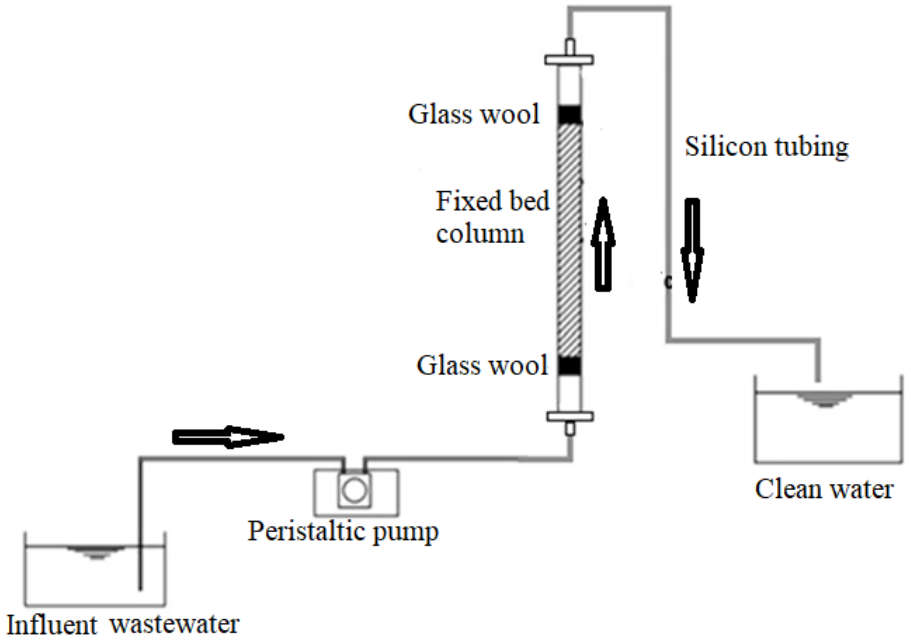

Figure 2: A sketch of the experimental setup for an up flow of effluent through the fixed bed column

The discharged samples were collected periodically. The optical densities of the crystal violet in the samples were determined using a UV–Vis spectrophotometer. Atomic absorption spectrophotometer (AAS) was used to determine the concentrations of metallic ions. Thomas model equation was used to evaluate multi–pollutants adsorption capacity of the SBF and SBF–MWCNTs.

Various conditions such as column height, flow rate, pH, MWCNTs:SBF mass ratios and initial concentrations were used to study the column adsorption capacity. The influence of bed height on the adsorption capacity was done by varying the height of the column from 4 cm to 12 cm while other variables were kept constant. The influence of MWCNTs in adsorption performance work was carried out by varying percentages of MWCNTs in SBF while maintaining other factors. The flow rate effect on adsorption capacity experiments was performed at flow rate range from 2.5 mL min^{-1} to 15 mL min^{-1} while other factors were kept constant. Initial concentration effect on the adsorption performance experiments was done by varying initial concentrations of solutions containing Cd^{2+}, Cr^{3+}, Pb^{2+}, Co^{2+} and CV by serial dilution of stock solution, from which working concentrations ranging from 6 ppm to 40 ppm was obtained. The effluents with pH ranging from 2.3 to 10.6 were used to study the effect of pH on multi–pollutants adsorption. One-way ANOVA statistical tool at 0.05 significance level was used to analyse the mean of three adsorption capacities of each contaminant between SBF and SBF-MWCNT adsorbents at optimum conditions.

Results and Discussion

Characterization of SBF based adsorbent

The percentage yield of SBF from the SB was 57 ± 7.09 %. The FT–IR spectra of the obtained SB and the extracted SBF are shown in Figure 3. The absorption peak at 1730 cm^{-1} of SB powder corresponds to C=O stretching of lignin, which is absent in the SBF spectrum. Also the peak at 1502 cm^{-1} corresponds to C=C aromatic stretch in phenolic group of lignin; does not exist in the SBF spectrum. This implies that delignification of SB using alkaline H_2O_2 was successful since the SBF did not show FT–IR signals corresponding to lignin. Modification

of the SBF with MWCNTs give new FT–IR band observed at 1639, which Dillon et al. (2000) attributed it to MWCNTs vibrational modes. There was reduction of O–H stretch band intensity at 3333 cm^{-1} that corresponds to cellulose and hemicellulose.

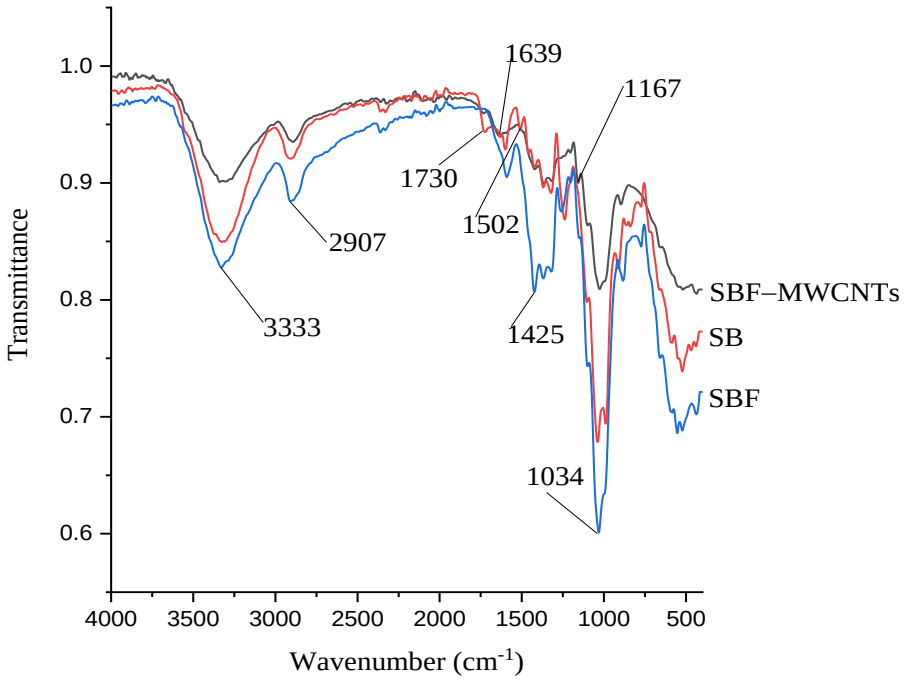

Figure 3: FT-IR spectra of SB, SBF and SBF–MWCNTs

The Boehm titration of SBF–MWCNTs composite containing 2% MWCNTs gave the total percentage acidic and basic groups of 68.7% and 31.3%, respectively, with increasing acidic groups from 0.720 of SBF to 1.747 of SBF–MWCNTs composite (Table 1). The improvement in surface acidic groups lowers the point of zero charge (pHpzc) that resulting to increasing of negative charge on the adsorbent's surface and enhance electrostatic interaction with cationic dyes (Shabaan et al. 2020, Konicki and Pełech 2019).

Table 1: Total basic and acidic groups of the SBF–MWCNTs

Biosorbent	Total basic groups (mmol g^{-1})	Total acidic groups (mmol g^{-1})	Basic and acidic groups (mmol g^{-1})	% Acidic groups	% Basic groups
SBF	0.814	0.720	1.534	46.9	53.1
SBF–MWCNTs	0.797	1.747	2.544	68.7	31.3

From XRD peaks shown in Figure 4, the key crystalline peaks at 2θ degree of 22.1°, 23.5° and 29.4° corresponds to SBF (Park et al. 2010). After modifications with MWCNTs there was increase in intensities of the peaks at 22.1° and 23.5°, while a peak at 29.4° diminished. Also, there was a new peak observed at 26.6° which was associated with

MWCNTs (Nie et al. 2015). Percentage Crystallinity Index (CI) of the materials was obtained as described elsewhere (Park et al. 2010).

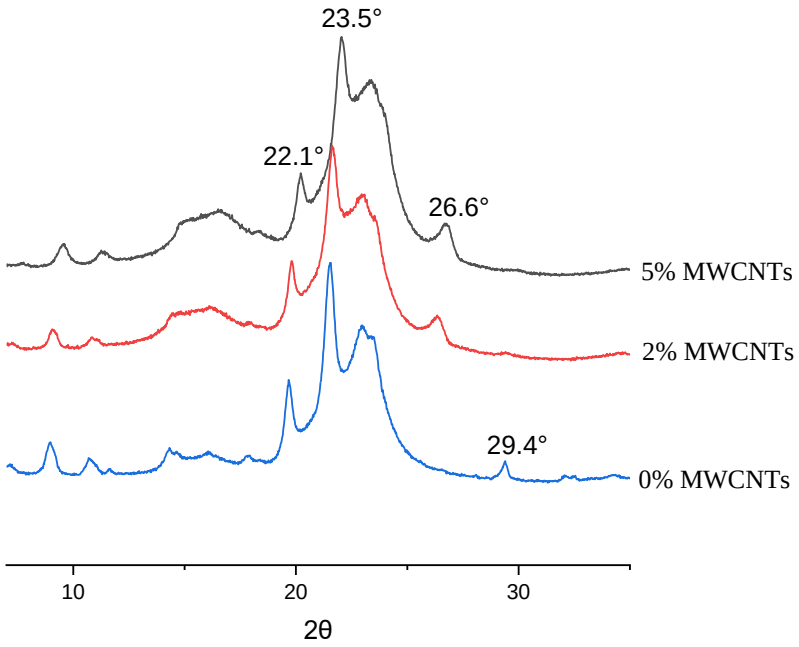

Figure 4: XRD spectra of SBF containing different amounts of MWCNTs

The CI values were calculated using Equation 1 as the ratio of the integrated area of all crystalline peaks (sharp peaks) to the total integrated area under the XRD peaks (sharp plus broad peaks).

$$CI = \frac{\text{Integrated area of all crystalline peaks}}{\text{Total integrated area under the XRD peaks}} \times 100 \qquad (1)$$

The obtained CI values were plotted as a function of percentage of MWCNTs incorporated in SBF (Figure 5). As shown in Figure 5, the percentage crystallinity index ranged from 69.83% (SBF) to over 70.7% (2% MWCNTs in SBF). With more than 2% MWCNTs the composite's crystallinity remained almost the same.

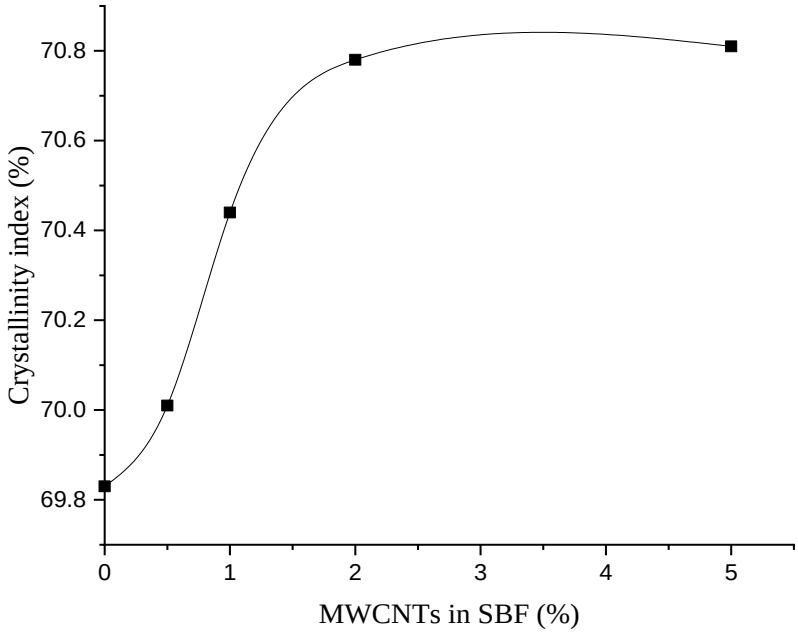

Figure 5: A plot of percentage CI as a function of percentage of MWCNTs incorporated in SBF

Since MWCNTs are more crystalline, as expected, blending with SBF caused the crystallinity index of the SBF–MWCNTs to increase. As seen from Figure 5, the CI of SBF–MWCNTs reached climax with 2% addition of MWCNTs to SBF. Further addition of MWCNTs did not significantly influence the CI of SBF–MWCNTs because the CI of the composite material approached that of pure MWCNTs (70.9%) (Yang et al. 2008).

Solvent swelling ratio, S_r, defines the amount of solvent held innately by the sorbent. Swelling ratios of SBF and SBF–MWCNTs were calculated from the mass of swollen sorbent material, M_s, and mass of dry sorbent material, M_o, using Equation 2.

$$S_r = \frac{M_s - M_o}{M_o} \qquad (2)$$

The obtained S_r values were plotted as a function of percentage of MWCNTs incorporated in SBF (Figure 6).

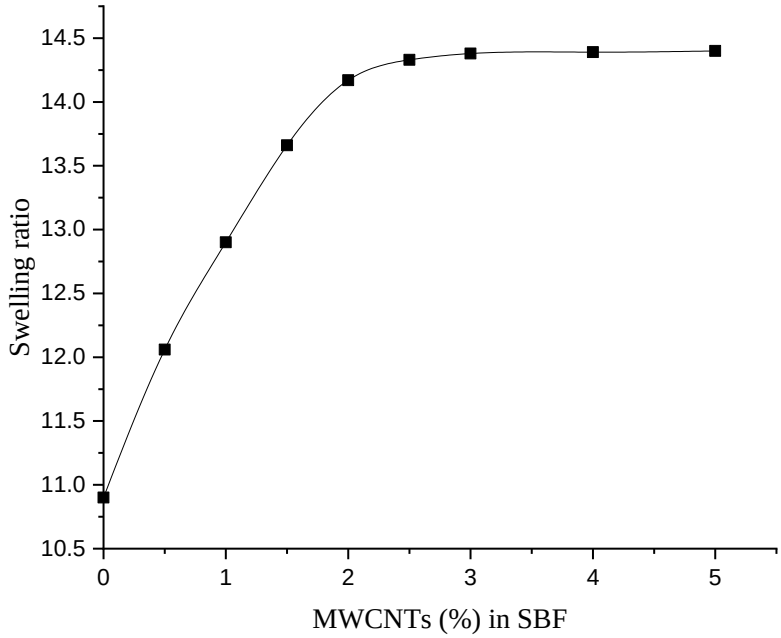

Figure 6: Swelling ratio of SBF–MWCNTs at different percentages of MWCNT in SBF

As can be observed from Figure 6, there was an increase in swelling ratio with increasing amount of MWCNTs in SBF up to 2%. Further increase in the amount of MWCNTs did not considerably result in the increase swelling ratio of the materials. As cited elsewhere (Kilulya 2018), swelling ratio plays an important role in the binding ability of the sorbent and enhances accessibility of active sites by improving diffusion rate of contaminants to the adsorbent. Therefore, it was thought that swelling increases adsorption capacity, since adsorption is controlled by diffusion of adsorbate to the adsorbent.

The TGA and DTG plots (Figure 7) at around 50–100 °C showed thermal events related to loss of water.

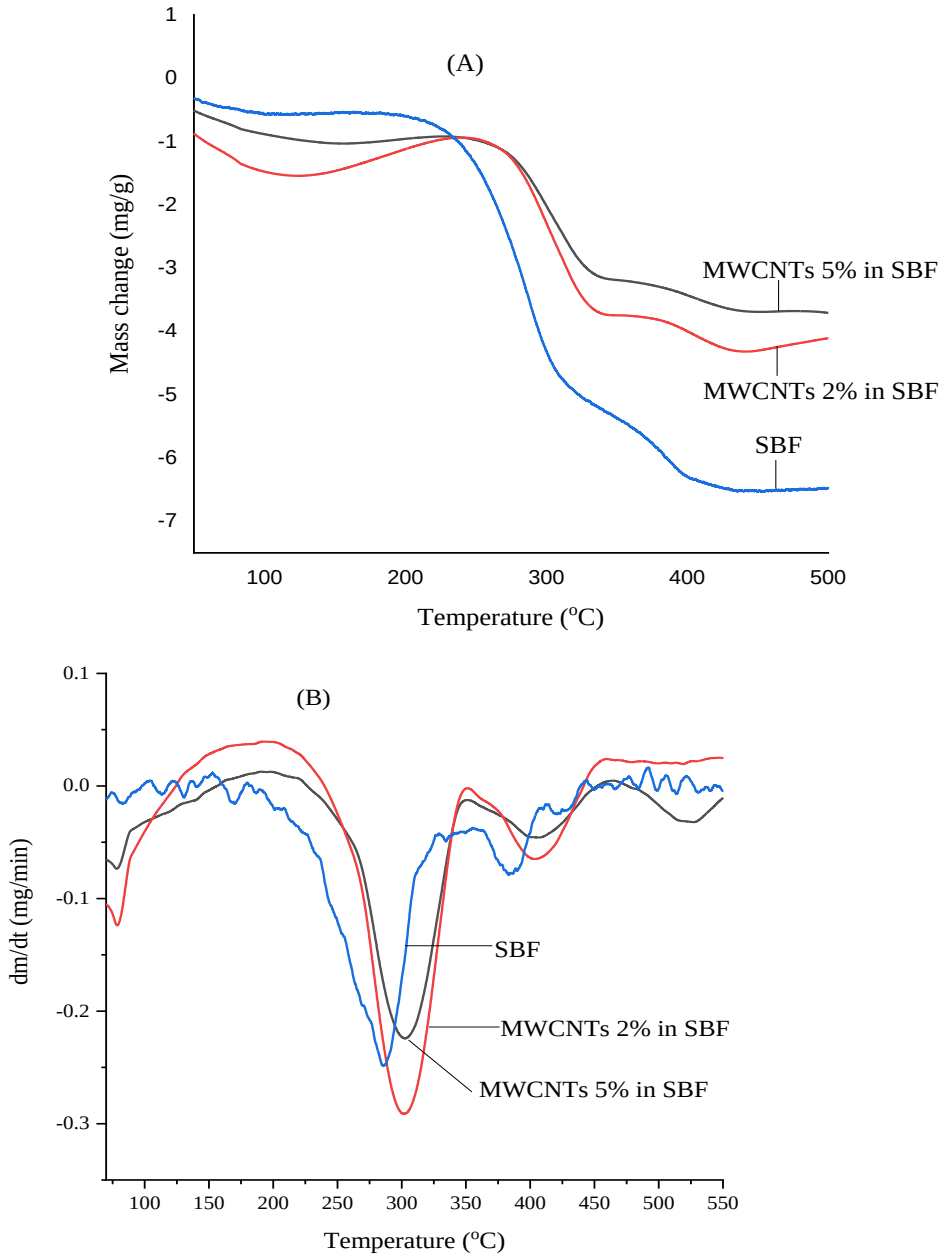

Figure 7: TGA (A) and DTG (B) curves of SBF and SBF modified with 2% and 5% MWCNTs

The unmodified SBF shows two main thermal degradations: the first one at 170 °C to 330 °C (Figure 7 A) whereby the DTG show the degradation peak at 285 °C (Figure 7 B). This is related to the decomposition both amorphous cellulose and hemicellulose. The second decomposition commenced at 360 °C to 410 °C (Figure 7 A) with DTG peak at 384 °C (Figure 7 B), representing the degradation of crystallite cellulose. These results are in line with findings reported in the literature (Poletto 2016). In addition, the

2% MWCNTs in SBF–MWCNTs composite showed two main thermal degradations. The TGA showed the first decomposition at 225 °C to 350 °C (Figure 7 A) with DTG peak at 304 °C (Figure 7 B), corresponding with the degradation of hemicellulose and amorphous cellulose. The next main degradation is for crystallite cellulose which appeared between 350 °C to 450 °C (Figure 7 A) whereby DTG peak found at 405 °C (Figure 7 B) (Bhuiyan et al. 2013). With 5% MWCNTs in SBF the TGA plot showed similar characteristics as the one with 2% MWCNTs with minor DTG peak shift amplification. Therefore, addition of MWCNTs to SBF shows the improvement of thermal stability of the composite materials, where by beyond 2% MWCNTs in SBF, the thermal stability change was not distinct.

Table 2 shows the average pore size and specific surface area of SBF and SBF–MWCNTs. One can see from this table that the average pore size and specific surface area of the SBF and SBF–MWCNTs ranged from 1.697 nm to 1.788 nm and 678.5 m^2 g^{-1} to 837 m^2 g^{-1}, respectively.

Table 2: Surface area and pore size of the fibres

Biosorbent	**Surface area (m^2 g^{-1})**	**Total pore volume mL g^{-1}**	**Pore size (nm)**
SBF	679	0.6642	1.697
MWCNTs (0.5) in SBF	730	0.7254	1.722
MWCNTs (1%) in SBF	768	0.7679	1.746
MWCNTs (1.5%) in SBF	794	0.8081	1.763
MWCNTs (2%) in SBF	815	0.8282	1.780
MWCNTs (2.5%) in SBF	821	0.8354	1.785
MWCNTs (3%) in SBF	829	0.8411	1.786
MWCNTs (4%) in SBF	834	0.8506	1.787
MWCNTs (5%) in SBF	837	0.8529	1.788

Additionally, it can be observed from Table 2 that addition of MWCNTs to SBF increased the surface area of the composite material. However, there was no significant increase of surface area and pore size with more than 2% of MWCNTs in SBF. Brunauer–Emmett–Teller (BET) adsorption-desorption isotherm plots of SBF and SBF-MWCNTs composite are shown in Figure 8. The plots structure is comparable to the one of cellulose based adsorbents reported by Kodali et al. (2021) which suggested the presence of micropores. Micropores are characterized with pore size less than 2.0 nm as shown in Table 2. According to Saleem et al. (2019); for a biosorbent to be used as a commercial grade, the surface area should be $\geq$ 500 m^2/g. This means that both modified and unmodified fibres registered sufficient surface area for adsorption of pollutants. However, the modified biosorbent showed improved surface area, therefore likely to have increased pollutant adsorption capacity.

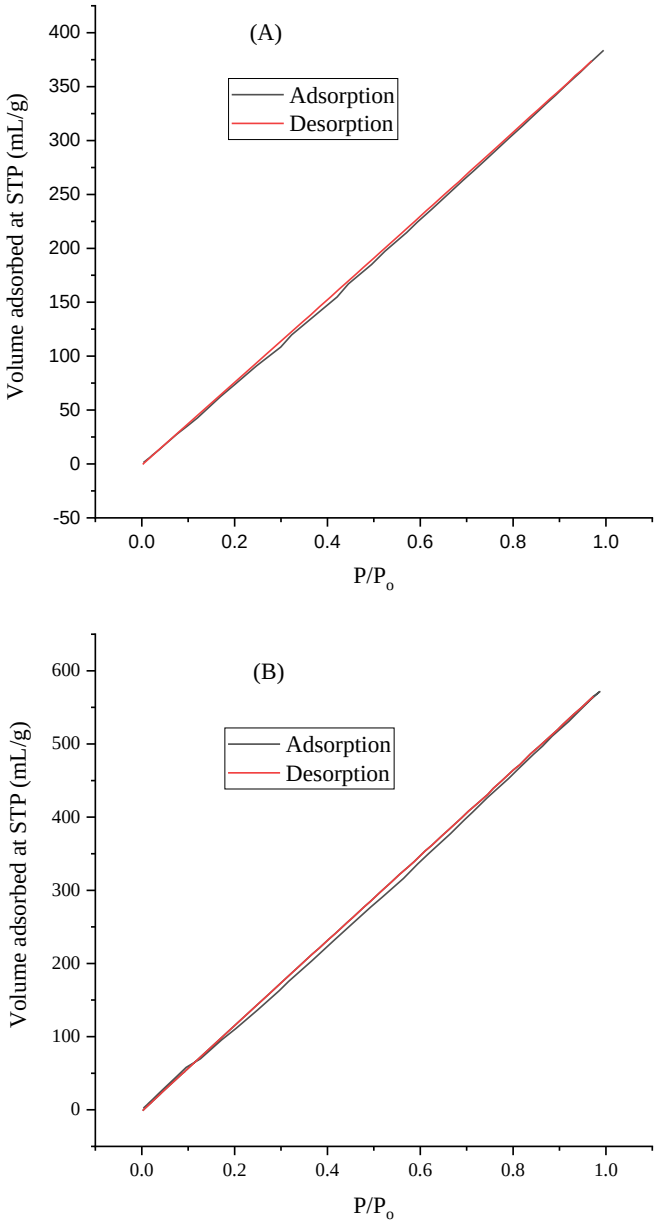

Figure 8: BET isotherms of SBF (A) and SBF–MWCNTs composite (B)

Adsorption studies of the SBF based adsorbent

According to theory (Patel 2019), the dynamic behaviour of fixed bed column is described in terms of an ‘‘effluent concentration-time’’ profile, which is called the breakthrough curve. In the fixed bed method, Thomas model linear Equation 3 is useful in the determination of adsorption capacity (Biswas and Mishra 2015).

$$\ln\left(\frac{C_o}{C_e}-1\right)=\frac{K_T q_o M}{Q}-K_T C_o t \qquad (3)$$

where C_o is inlet concentration; C_e is effluent concentration; K_T is Thomas rate constant (mL min^{-1} mg^{-1}); q_o is adsorption capacity (mg g^{-1}); M is total mass of the adsorbent (g);

Q is volumetric flow rate (mL min^{-1}). Then the plot of $\ln\left(\frac{C_o}{C_e}-1\right)$ versus time (t) gives a straight line with slope of $K_T C_o$ and intercept of $\frac{K_T q_o M}{Q}$. From the intercept, the adsorption capacity (q_o) can be calculated. Figure 8 show a sample plot used to determine adsorption capacity of Pb(II) at bed height of 12 cm, initial concentration of about 30 mg/L, pH of 7.04, and flow rate of 2.5 mL/min.

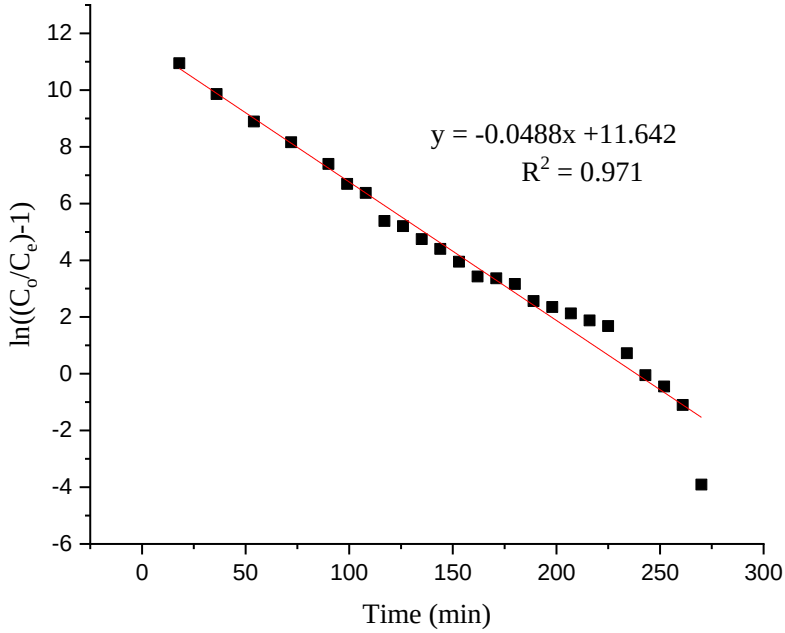

Figure 9: Plot of $\ln\left(\frac{C_o}{C_e}-1\right)$ against time used to determine adsorption capacity

From Figure 9, the values of Thomas rate constants and adsorption capacity were found to be 1.63 mL min^{-1} mg^{1} and 7.98 mg g^{-1}, respectively. This adsorption capacity value belongs to Pb(II) at 12 cm bed height in Figure 10. All other adsorption capacity values were determined in the same way, except at different conditions, i.e., bed height, flow rate, pH, pollutant initial concentration and SBF:MWCNTs ratio. The results are summarised in Figure 10.

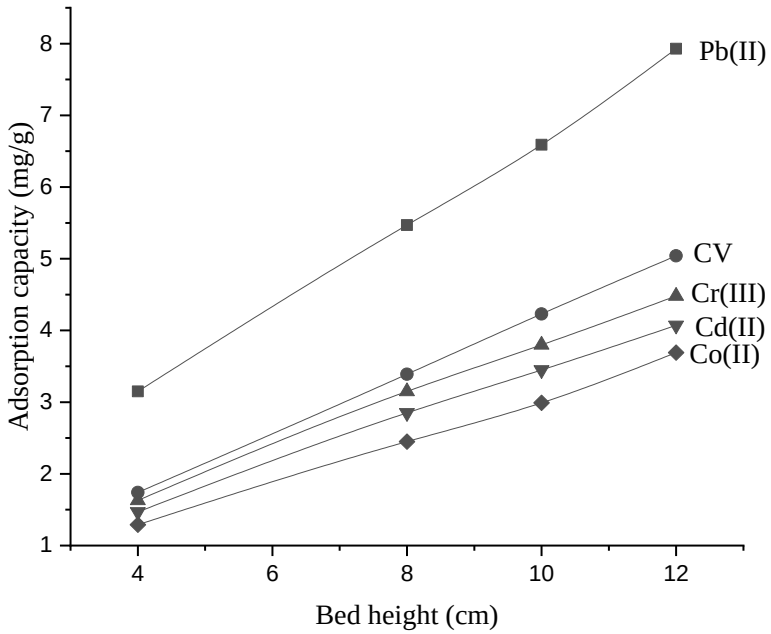

Figure 10: Effect of bed height on the adsorption capacity

As shown in Figure 10, when other parameters were kept constant, the increase in bed height resulted to increase adsorption capacity of all studied pollutants. Adsorption capacity of Pb(II) was higher compared to other pollutants at all bed heights, followed by CV, Cr(III), Cd(II) and Co(II), in that order. The CV adsorption capacity was the second higher next to Pb(II). This may be attributed to the presence of additional functional groups in the adsorbent due to modification with MWCNTs, which favours cationic dyes adsorption (Konicki and Pelech 2019).

The increase in bed height means increase in amount of adsorbent material, hence a greater number of active sites. Also, axial dispersion is more pronounced at low bed depth in case of mass transfer, which causes slow diffusion of the adsorbate from the liquid to the solid phase which is contrary at higher bed height. Additionally, the time taken by the adsorbates to move through the column is longer with a higher bed height. Therefore, the contact time between the contaminants and the surface active sites of the adsorbent increases (Juela et al. 2021).

Influence of MWCNTs percentage in SBF

A plot of adsorption capacity of contaminants as a function of the increase in amount of MWCNTs in SBF is presented in Figure 11. As observed in this figure, the pollutant adsorption capacity of the adsorbent increased slightly up to 2% of MWCNTs. The improved adsorption performance with addition of MWCNTs is related to increased surface area and swelling ratio of the material.

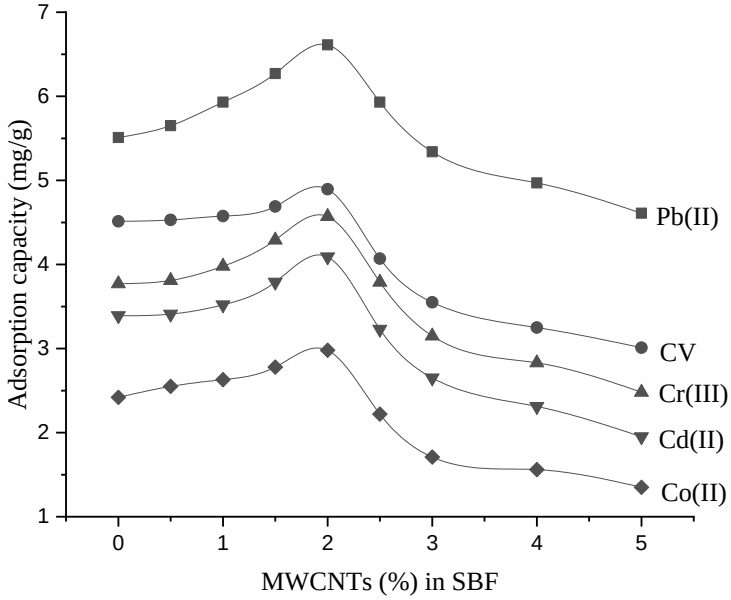

Figure 11: Effect of MWCNTs increase in the SBF–MWCNTs adsorbent performance

It can also be seen from this figure that beyond 2% of MWCNTs the adsorption performance of the SBF–MWCNTs decrease. This is because MWCNTs have limited number of potential functional groups for pollutants sequestration, thus further increase of MWCNTs in the composite material decrease its adsorption capacity (Datsyuk et al. 2008). Figure 12 shows the adsorption performance comparison between SBF and SBF-MWCNTs. Statistical treatment of data using One-way ANOVA at 0.05 significance level show that, the mean adsorption capacity of each contaminant in 2% SBF-MWCNTs is significant higher than that in SBF.

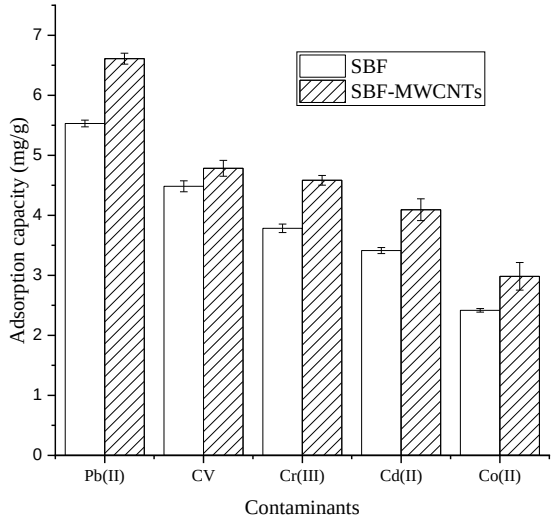

Figure 12: Comparison of mean adsorption capacities of contaminants between SBF and SBF–MWCNTs adsorbents (n = 3)

Effect of flow rate

The influence of flow rate in the pollutants adsorption capacity of the column is shown in Figure 13. As shown in the figure, the column performance in removal of contaminants decreases with increasing flow rate.

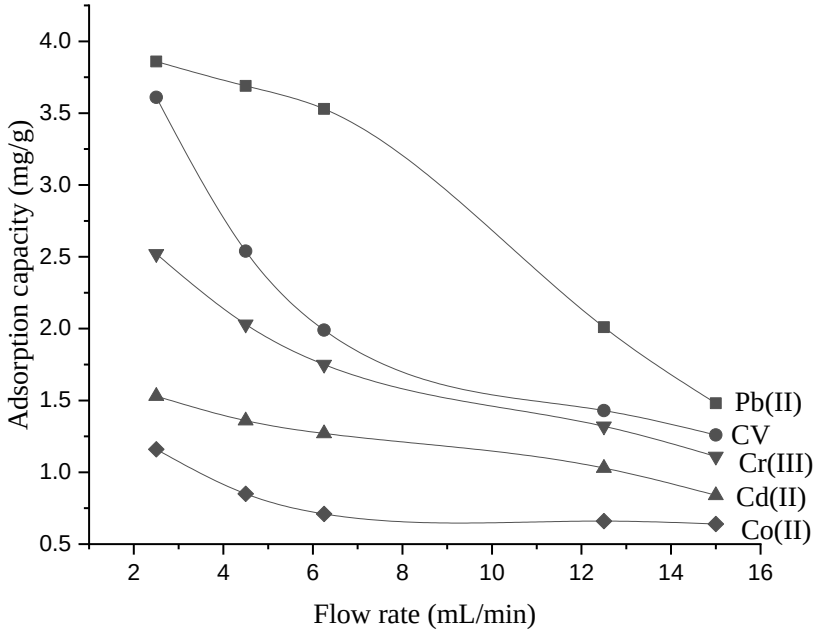

Figure 13: The effect of flow rate in the SBF–MWCNTs column performance

In addition, adsorption of Pb(II) was much affected by effluent flow rate. Change in flow rate from 2.5 to 15 mL/min reduced the adsorption capacity of Pb(II) by about 2.4 mg g^{-1}. Adsorption capacity of Co(II) was the poorest in all flow rates tested and was the least affected by increase in flow rate. Decrease in pollutants adsorption capacity with increasing flow rate can be attributed to decrease in contact time between pollutants and the adsorbent. At low flow rate adsorbates get sufficient time to explore and bind to active sites of the biosorbent, which is contrary to fast flow rate (Priya and Radha 2015). Thus, the breakthrough and saturation times are greater at lower flow rates. Juela et al. (2021) proposed that high flow rates tend to cause turbulence within the interstitial spaces of the bed, and this turbulence increases the possibility of dispersal effects, thus impeding the uptake of pollutants into the pores of SBF–MWCNTs.

Influence of initial concentration

Figure 14 shows the effect of initial pollutant concentration on the efficacy of the column to uptake the pollutants.

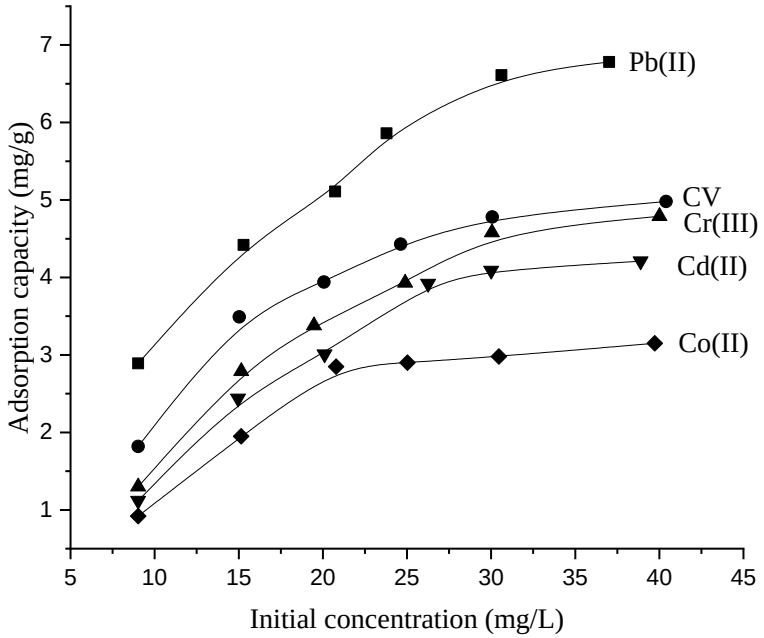

Figure 14: Effect of initial concentration on adsorption capacity

From this figure, one can perceive that the adsorption capacity of each contaminant increases with increase in its respective initial concentration. However, at the pollutant concentrations ≥25 mg/L the increase of pollutants adsorption capacity was insignificant. Since adsorption of pollutants on the adsorbent surface is controlled by the equilibrium of the contaminants between the solution and the adsorbent surface, then as the contaminants concentration increases in the solution the equilibrium shifts towards the adsorbent and the number of collisions between contaminants and the adsorbent increases. As a result, the adsorption capacity is improved until all the active sites are saturated (Amel et al. 2012). The results from this study recommend the initial pollutant concentrations of ≤25 mg/L for a better column performance.

Effect of pH on the biosorption process

The effect of pH on the adsorption capacity of the column is presented in Figure 15. As can be seen from this figure, adsorption capacity of the column increases sharply with an increase in pH up to 5.5. Above this pH, the adsorption capacity of the column did not increase considerably. This means that the best working pH should be adjusted to >6. At lower pH the removal of contaminants was low due to the high concentration of H^+ which competes with metal ions and crystal violet for the active sites (Feng et al. 2011). As the pH increases, more active sites become accessible because the competition of H^+ and the pollutants is reduced (Kulkarni et al. 2017).

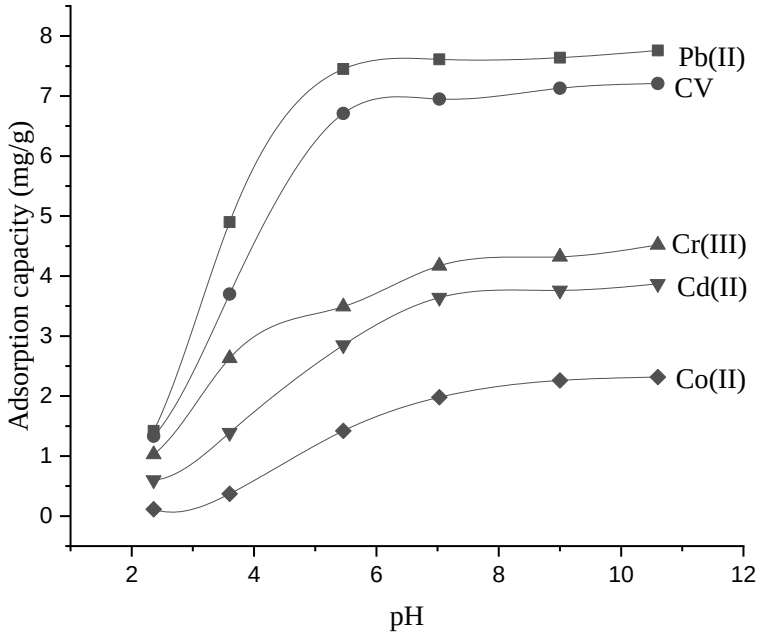

Figure 15: The effect of pH in adsorption performance of SBF–MWCNTs

Conclusions

The percentage yield of fibres from the sugarcane bagasse was found to be 57 ± 7.09 %. The delignification of sugarcane bagasse using alkaline H_2O_2 was successful since the obtained fibres did not display FT–IR signals corresponding to lignin. The Boehm titration of SBF–MWCNTs composite containing 2% MWCNTs gave the total percentage acidic and basic groups of 68.7% and 31.3%, respectively. The maximum percentage crystallinity index of over 70.7% was registered by the SBF–MWCNTs composite containing 2% MWCNTs. The composite containing 2% MWCNTs gave the highest swelling ratio, thermal stability, and surface area. The pore sizes of the composite containing 2% MWCNTs were micropores (<2.0 nm). As expected, the increase in bed height caused an increase in the adsorption capacity of the pollutants. The best adsorption capacity of the pollutants was registered using composite containing 2% of MWCNTs. It was also established that lower flow rates give a greater breakthrough and saturation times. A better column performance was recorded with the initial pollutant concentrations of ≤25 mg/L and pH >6. Therefore, the SBF–MWCNTs composite containing 2% MWCNTs is a promising candidate for simultaneous removal of multi–pollutants from industrial wastewaters.

Acknowledgements

The authors thank the International Science Programme (ISP) for partial financial support used during characterization of materials via Materials Science and Solar Energy Network for Eastern and Southern Africa (MSSEESA).

References

Al-Azabi K, Al Marog S, Abukrain A, Sulyman M 2018 Equilibrium, isotherm studies of dye adsorption onto orange peel powder. *Chem. Res. J.* 3:45-59.

Akhtar N, Syakir Ishak, MI, Bhawani SA, Umar K 2021 Various natural and anthropogenic factors responsible for water quality degradation: A review. *Water*.13: 1-35.

Amel K, Hassen AM, Kerroum D 2012 Isotherm and kinetics study of biosorption of cationic dye onto banana peel. *Energy Proc* 19:286-295.

Bhuiyan KH, Rahman M, Mina F, Islam MR, Gafur A, Begum A 2013 Crystalline morphology and properties of multi-walled carbon nanotube filled isotactic polypropylene nanocomposites: Influence of filler size and loading. *Composites A.* 52:70-79.

Biswas S, Mishra U 2015 Continuous fixed-bed column study and adsorption modelling: removal of lead ion from aqueous solution by charcoal originated from chemical carbonization of rubber wood sawdust. *J Chem.* 2015:1-9.

Choi SY, Park K-Y, Kim HJ and Kweon JH 2015 Removal of heavy metal and nitrate nitrogen in polluted groundwater by electrodialysis process. *J. Water Resource Hydraul. Eng*. 4: 1-1.

Datsyuk V, Kalyva M, Papagelis K, Parthenios J, Tasis D, Siokou A, Kallitsis I, Galiotis C 2008 Chemical oxidation of multiwalled carbon nanotubes. *Carbon,* 46:833 –840.

Dillon AC, Gennett T, Alleman JL, Jones KM, Parilla PA, and Heben MJ 2000 Carbon nanotube materials for hydrogen storage. *Proceedings of the 2000 Hydrogen program review*. pp 1–20.

Dingenen J 1998 Columns and packing methods. *Analusis magazine,* 26: 18-33.

Fang Z, Wu P-Y, Lin Y-N, Chang T-H, Chiu Y-h 2021 Air pollution's impact on the economic, social, medical, and industrial injury environments in China. *Healthcare* 9: 1-21.

Feng N, Guo X, Liang S, Zhu Y and Liu J 2011 Biosorption of heavy metals from aqueous solutions by chemically modified orange peel. *J. Hazard. Mat.* 185: 49-54.

Ghurye GL, Mishra D and Lucas L 2012 Thermal desalination of produced water: an analysis of the partitioning of constituents into product streams and its implications for beneficial use outside the O&G Industry. *Water,* 13:1- 25.

Hezarjaribi M, Bakeri G, Sillanpää M 2021 Novel adsorptive PVC nanofibrous/thiol-functionalized TNT composite UF membranes for effective dynamic removal of heavy metal ions. *J. Environ. Manag. 284*:1-16.

Hossain MA and Hossain ML 2014 Kinetic study of Malachite Green adsorption on used black tea leaves from aqueous solution. *Int J Adv Res*, 2: 360-374.

Juela D, Vera M, Cruzat C, Alvarez X and Vanegas E 2021 Adsorption properties of sugarcane bagasse and corn cob for the sulfamethoxazole removal in a fixed-bed column. *Sus. Env. Res.* 2021: 1-14.

Kaleta J, Papcia D, Puszkarewicz A 2018 Using ion exchange process in removal of selected organic pollution from aqueous solutions. *J. Ecol. Eng*. 19: 136–142.

Kilulya KF 2018 Preparation, characterisation and application of molecularly imprinted polymers for the selective removal of sterols from water. *Tanz. J. Sci.* 44: 27-44.

Kodali J, Arunraj B, Sathvika T, Kumar ASK and Nagarathnam R 2021 Prospective application of diethylaminoethyl cellulose (DEAE-cellulose) with a high adsorption capacity toward the detoxification of 2,4-dichlorophenoxyacetic acid (2,4-D) from water. *RSC Adv.*11:22640–22651.

Konicki W, Pełech I 2019 removing cationic dye from aqueous solutions using as-grown and modified multi-walled carbon nanotubes. *Pol. J. Environ*. 28: 717–727.

Kulkarni MR, Revanth T, Acharya A and Bhat P 2017 Removal of Crystal Violet dye from aqueous solution using water hyacinth: Equilibrium, kinetics and thermodynamics study. *Resource-Efficient Technologies* 3: 71–77.

Liu C, Ding Y, Wu W 2016 A simple and effective strategy to fast remove chromium (VI) and organic pollutant in photoelectrocatalytic process at low voltage. *Chem. Eng. J. 306*: 22–30.

Lopera AE-E, Ruiz SG, Alonso JMQ 2019 Removal of emerging contaminants from wastewater using reverse osmosis for its subsequent reuse: Pilot plant. *J. Water Proc.engineering.*29: 1-10.

Ma'ruf A, Pramudono B, Aryanti N 2017 Lignin isolation process from rice husk by alkaline hydrogen peroxide: lignin and silica extracted. *AIP Conference Proceedings* 1823: 1-5.

Nie P, Min C, Song H-J, Chen X, Zhang Z, Zhao K 2015 Preparation and tribological properties of polyimide/carboxyl-functionalized multi-walled carbon nanotube nanocomposite films under seawater lubrication. *Tribol Lett.* 58: 1-12.

Obinnaa IB and Ebere EC 2019 Water pollution by heavy metal and organic pollutants: Brief review of sources, effects and progress on remediation with aquatic plants. A review: *Anal. Methods Environ. Chem. J*. 2: 5-38.

Ong P-S, Ong S-T and Hung Y-T 2013 Utilization of mango leaf as a low-cost adsorbent for the removal of Cu(II) ions from aqueous solution. *Asian J. Chem.* 25: 6141-6145.

Park S, Baker JO, Himmel ME, Parilla PA and Johnson DK 2010 Research Cellulose crystallinity index: measurement techniques and their impact on interpreting cellulase performance. *Biotechnol Biof*. 3:1-10.

Patel H 2019 Fixed-bed column adsorption study: Review. *Appl. Water Sci.* 9: 1-17.

Patil S, Deshmukh V, Renukdas S, Patel N 2011 Kinetics of adsorption of crystal violet from aqueous solution using different natural materials. *Int.J. Env. Sci*, 1**:** 1123-1141.

Pohl A 2020 Removal of heavy metal ions from water and wastewaters by sulfur-containing precipitation agents. *Water Air Soil Pollut.* 231:1-17.

Poletto M 2016 Effect of extractive content on the thermal stability of two wood species from Brazil. *Maderas-cienc Tecnol.* 18: 435 – 442.

Priya SS, Radha KV 2015 Fixed-bed column dynamics of tetracycline hydrochloride using commercial grade activated carbon: comparison of linear and nonlinear mathematical modeling studies. *Desalin. Water Treat.* 2015:1-17.

Rincòn GJ, Motta EJL 2014 Simultaneous removal of oil and grease, and heavy metals from artificial bilge water using electrocoagulation/flotation. *J Environ Manage*. 144:42–50.

Saleem J, Shahid UB, Hijab M, Mackey H, McKay G 2019 Production and applications of activated carbons as adsorbents from olive stones. *Biomass Convers. Biorefin.* 9:775–802.

Shabaan OA, Jahin HS, Mohamed GG 2020 Removal of anionic and cationic dyes from wastewater by adsorption using multiwall carbon nanotubes. *Arab. J. Chem.*13: 4797-4810.

Shrestha B, Homagai PL, Pokhrel M R, Ghimire KN 2012 Exhausted Tea Leaves – a low cost bioadsorbent for the removal of Lead (II) and Zinc (II) ions from their aqueous solution, *J. Nepal Chem. Soc.* 30:123-129.

Yang K, Han H, Pan X, Chen N and Gu M 2008 The effect of chemical treatment on the crystallinity of multi-walled carbon nanotubes. *J. Phys. Chem. Sol.* 69: 222–229.